Inhibition of neuroinflammatory nitric oxide signalling supresses protein glycation and recovers neuronal dysfunction in prion disease

Julie-Myrtille Bourgognon
University of Glasgow School of Life Sciences
Jereme G. Spiers
La Trobe University
Sue Robinson
MRC Toxicology Unit
Hannah Scheiblich
Universitat Bonn Mathematisch-Naturwissenschaftliche Fakultat
Catharine Ortori
University of Nottingham
Sophie J. Bradley
University of Glasgow School of Life Sciences
Andrew B. Tobin
University of Glasgow School of Life Sciences
Joern Steinert (js333@le.ac.uk)
University of Leicester Medical School https://orcid.org/0000-0003-1640-0845

Research article

Keywords: neurodegeneration, nitric oxide, neuroinflammation, glycation, prion aggregation, synapse function

Posted Date: April 9th, 2020

DOI: https://doi.org/10.21203/rs.3.rs-20075/v1

Abstract

Background: Several neurodegenerative diseases associated with protein misfolding (Alzheimer's, Parkinson's disease) exhibit oxidative and nitrergic stress following initiation of neuroinflammatory pathways. Associated nitric oxide (NO)-mediated post-translational modifications impact upon protein functions that can exacerbate pathology. Non-enzymatic and irreversible glycation signalling has been implicated as an underlying pathway that promotes protein misfolding, but the direct interactions between both pathways are poorly understood.

Methods: Here we investigated the potential therapeutic effects of supressing neurotoxic NO signalling during early progression of prion disease. Tg37 mice aged 3-4 weeks were inoculated by intracerebral injection with either 1% brain homogenate of Rocky Mountain Laboratory (RML) scrapie prion protein or control normal brain homogenate (NBH). Hippocampal gene and protein expression levels of oxidative and nitrergic stress markers were analysed and electrophysiological characterisations of pyramidal neurons were performed in 6-10 weeks old RML and NBH mice. Mice were injected with a NO synthase (NOS) inhibitor and the time course of disease markers was compared to controls. Electrophysiology, immunoblotting and immunocytochemistry studies were performed to identify the effects of NOS inhibition on neurophysiology, glycation, prion protein misfolding and cell death. Statistical analyses employed two-tailed unpaired Student's *t*-test, one-way or two-way ANOVA as required and data were considered significant with $P<0.05$.

Results: Increased neuroinflammatory signalling was observed in mice between 6 and 10 weeks post inoculation (w.p.i.) with scrapie prion protein which was characterised by enhanced nitrergic stress and associated with a decline in hippocampal neuronal function by 9 w.p.i.. Daily *in vivo* administration of the NOS inhibitor L-NAME between 6 and 9 w.p.i. at 20 mg/kg abolished the functional degeneration of hippocampal neurons in prion mice. We further found that this intervention in diseased mice ameliorated 3-nitrotyrosination of triose-phosphate isomerase, an enzyme involved in the formation of disease-associated glycation signalling. Furthermore, L-NAME application reduced the expression of the receptor for advanced glycation end products and the accumulation of hippocampal prion misfolding.

Conclusions: Our data suggest that alleviating nitrergic stress during early phases of neurodegeneration reduces neurotoxic post-translational NO signalling and glycation-assisted prion misfolding in the hippocampus, a mechanism which might be applicable to other protein misfolding neurodegenerative conditions.

Background

Diseases associated with old age, including Alzheimer's disease (AD) and other forms of dementia, are increasing in prevalence and, although symptomatic treatments exist, no cure to prevent the progression has yet been described. Neurodegenerative diseases associated with the accumulation of misfolding

proteins including AD, Parkinson's disease (PD) and various forms of prion disease share many common features such as upregulation of neuroinflammatory signalling [1]. In particular, neuroinflammatory signalling can compromise synaptic plasticity [2] in early degeneration representing an initiation phase for dysfunction. It is well established that cellular stress signalling in neurodegenerative diseases is associated with aberrantly elevated levels of nitric oxide (NO) and activation of oxidative/nitrergic stress pathways [3-5]. NO has both physiological and pathological roles in the nervous system where it is synthesized by NO synthases (neuronal NOS [nNOS], inducible NOS [iNOS] and endothelial NOS [eNOS]). Excessive NO production reported in prion disease, AD and PD is leading to aberrant post-translational protein modifications and unbalanced neurotoxic nitrergic signalling [6-9]. Protein cysteine residues can be directly and reversibly S-nitrosylated by NO [9] which can lead to protein dysfunction to facilitate disease progression [10, 11]. NO also reacts with free radicals such as superoxide anion O^{2-} resulting in the generation of peroxynitrite which accumulatively induces protein nitrotyrosination, the irreversible chemical addition of a nitro group to the tyrosine residues generating 3-nitrotyrosine (3-NT), which can result in a loss of physiological protein function [12]. Therefore, preventing disease-relevant, in particular, iNOS-mediated NO generation is a strong and promising therapeutic target across many neurological diseases [13-15].

In neurodegenerative conditions, oxidative and nitrergic stress is believed to be an initiator of many pathological pathways and can have both direct and indirect roles in the mechanisms underlying neurodegeneration [16-18]. For example, 3-nitrotyrosination of β-amyloid (Aβ) oligomers is thought to be one of these direct pathways by increasing oligomer stability and toxicity [12, 19]. Interestingly, Aβ42 oligomerisation also plays a key role by promoting nitrergic stress *i.e.* inducing 3-nitrotyrosination of neuronal proteins [20]. One of these targeted proteins is the enzyme triose-phosphate isomerase (TPI) which regulates the glycolytic flow by interconverting dihydroxyacetone phosphate (DHAP) and glyceraldehyde 3-phosphate (GAP). The nitrergic post-translational modification of TPI induced by the Aβ-peptide reduces its enzymatic activity [21] leading to a shift of balance of the metabolites towards DHAP formation. Subsequently, DHAP transforms spontaneously into the cytotoxic metabolic by-product methylglyoxal [22, 23]. A nitro-oxidative environment favours high levels of 3-nitrotyrosinated TPI in AD patients [21] and as a result, inhibition of this enzyme leads to non-enzymatic methylglyoxal-mediated generation of protein glycation [21] and formation of advanced glycation end products (AGE).

The production of AGE is irreversible and glycated protein products have a propensity to aggregate [24] while exhibiting resistance to protease degradation. Notably, protein glycation is a marker of aging and it promotes inflammation *via* the overproduction of intracellular reactive oxygen species (ROS) in addition to impairing proteasomal activities. The resulting AGE-mediated induction of oxidative stress thereby leads to augmented oxidative damage in the brain presenting a positive feedback loop of neurotoxic pathways in different protein misfolding diseases [25-27]. In AD, the aggregation and deposition of AGEs have been observed in tau protein tangles and Aβ plaques [28, 29] with the polymerization of Aβ being significantly accelerated by AGE-mediated protein cross-linking [30]. Glycation at specific residues causes a profound impact on the ability to form amyloid fibrils [31, 32] confirming a contributing role of this

modification in aggregation. AGEs are principally recognised by the receptor for AGE (RAGE) that belongs to the immunoglobulin gene superfamily. RAGE is found on the surface of numerous cells types including microglia, monocytes, astrocytes, neurons and endothelial cells [33]. RAGE activation results in the stimulation of nicotinamide adenine dinucleotide phosphate (NADPH) oxidase [34], an enzyme that produces superoxide radicals. It also induces the production of cytokines *via* NF-kB expression, followed by upregulation of inflammatory pathways [33]. Importantly, AGE-formation and RAGE expression are increased in brains from Creutzfeldt Jakob Disease (CJD) patients and are associated with enhanced oxidative and nitrergic stress in patient brains [35, 36] suggesting the possibility that AGE-mediated modifications might, in part, play a role in the accumulation of the aberrant prion protein.

In this study, we investigated neurodegeneration induced by prion misfolding to assess the role of nitrergic stress caused by excess production of NO during the progression of the disease. We established that the decline of hippocampal CA1 pyramidal neuronal function is associated with increased nitrergic stress and reduced levels of antioxidants, and that prolonged *in vivo* treatment with a NOS inhibitor reduced prion protein aggregation and diminished aspects of neurodegenerative signalling such as functional neuronal decline. We further found that blocking NO signalling reduced nitrotyrosination of TPI and RAGE upregulation.

Methods

Mice and Prion inoculation

Hemizygous Tg37 mice that overexpress the cellular mouse prion protein (PrP^{C}) have been used as described previously [37]. Mice were fed *ad libitum* with a standard mouse chow. Tg37 mice aged 3 to 4 weeks were inoculated by intracerebral injection into the right parietal lobe with 1% brain homogenate of Rocky Mountain Laboratory (RML) misfolded prion protein (PrP^{Sc}) [37]. Control mice received 1% normal brain homogenate (NBH) and hippocampi and cortices' of both groups were used for analyses.

Animal drug treatment

Tg37 mice inoculated with NBH or RML brain homogenate are denoted as NBH or RML mice. RML mice were treated (*i.p.*) with vehicle (5% glucose) or N(ω)-nitro-L-arginine methyl ester (L-NAME, 20 mg/kg) daily from 6 weeks post inoculation (w.p.i.) for 3 weeks. This dosage provides a ~70% inhibition of lipopolysaccharide-induced NO_x generation (*via* iNOS induction) in mice with an ED_{50} for L-NAME of 5 mg/kg [38]. The presence of the L-NAME metabolite and active inhibitor of NOS in the brain, L-NOARG [39], was confirmed by high-performance liquid chromatography (HPLC) at a concentration of 11.8±1.1 nM/g tissue (n=8 mice).

Liquid chromatography–mass spectrometry (LC/MS) analysis of the metabolite

L-NAME was injected (20 mg/kg; *i.p.*) daily for 5 days to reach steady-state levels before the mice were sacrificed and the brains dissected and snap-frozen in liquid nitrogen. The tissue samples were weighed

still in the frozen state and disrupted using a micropestle in an Eppendorf tube. A two-stage extraction was performed to ensure denaturation, membrane disruption and extraction of the metabolite L-NOARG. A mix of chloroform/methanol (0.5 ml, 2:1) was added to the tubes and vortexed for 20 min. After centrifugation, the supernatant was removed to another Eppendorf tube and the pellets were re-suspended in 0.5 ml 50% methanol/water. They were again vortexed and re-centrifuged. The solvent mixes were pooled for each sample and then dried in a centrifugal evaporator. Samples were reconstituted in 100% methanol by vortexing and re-centrifugation. The HPLC system used was a modular LC Shimadzu LC system, equipped with pump, cooled autosampler and column oven at 45□C. A Phenomenex Gemini 18 3µ column 100x2mm was used at 45□C, with mobile phase A (0.01% formic acid (pH 4.6) in water) and mobile phase B acetonitrile. The compound was eluted on a gradient from 0.0% B to 60% B in 5 min with a 2 min wash at 100% B. The MS system used was a Sciex 4000 QTrap run in ES+ve MRM mode. Four MRM channels (220.143>87.000, 220.143>174.200, 220.143>59.100 and 220.143>70.200) were monitored to ensure specificity. Quantification was performed against a dilution series of the standard and the extraction efficiency was included in the calculations.

Western blotting

Mouse hippocampi were dissected into ice-cold phosphate-buffered saline (PBS) containing protease inhibitors and phosphatase inhibitors (Complete, Roche Diagnostics) and samples were flash-frozen in liquid nitrogen until further analysis. All the following procedures were then performed at 4□C. Frozen tissue was homogenised in ice-cold RIPA buffer (20 mM Tris (pH 7.4), 150 mM NaCl, 3 mM EDTA, and 1% Nonidet P-40) and 1 x protease inhibitor cocktail with a tissue homogenizer (IKA T10 *basic ULTRA-TURRAX*®). Total protein concentration was measured by the Bradford method (BioRad Protein assay kit). Primary antibodies were as following: complexin1/2, 1:2000, 122102 Synaptic Systems; Kv3.1, 1:2000, Alomone labs; synaptobrevin, 1:1000, ab77314 Abcam; synaptophysin, 1:1000, 5467, Cell Signaling; synapsin, 1:2000, ab64581, Abcam; SNAP-25, 1:1000, ab41726 Abcam; Munc 18, 1:1000, ab3451, Abcam; 3-NT, 1:5000, ab61342, Abcam; TPI, 1:1000, ab6671, Abcam; RAGE, 1:1000, ab3611, Abcam; ICSM35 1:1000, D-Gen Ltd; tubulin 1:5000, 2144, Cell Signaling; actin, 1:5000, ab8224, Abcam.

Immunocytochemistry

Mice were anaesthetised with 3% isofluorane (2l/min O_2) and transcardially perfused with 20 ml of ice-cold PBS, followed by 20 ml of ice-cold 4% PFA. Following fixation, brains were immediately removed, and further fixed overnight in 4% PFA at 4□C. Brains were processed in paraffin wax and sliced at 5 µM using a microtome. Following antigen retrieval, sections were washed in TBS + 0.1% triton X-100 and blocked for 2 hours at RT in TBS, 0.1% triton X-100, 10% goat serum and 5% BSA. Sections were incubated with an anti-PrP antibody (1:1000, ICSM35, D-Gen) to recognise preferentially PrP^{Sc} over PrP^{C}, an anti-GFAP (1:1000, ab134436, Abcam) or an anti-NeuN (1:1000, MAB377, Millipore). Sections were washed three times and incubated with Alexa Fluor fluorescent secondary antibody for 1 hour at RT in blocking buffer. Following three washes, slices were mounted in Vectorshield hardset mounting medium with/without DAPI (Santa Cruz). For cell number analysis, pyramidal neurons were counted in

hippocampal or cortical sections, normalised to area and data averaged from three brains per condition. All images were taken using a Zeiss LSM 510 META NLO microscope with ZEN 2009 software (Zeiss).

NADPH-diaphorase assay

Mice were anaesthetised and transcardially perfused with PBS then 4% PFA. The brain was removed and fixed for 24 h in PFA before being embedded in paraffin. Five μm sections were cut and deparaffinised before being incubated in a mixture of 2.5 mg nitroblue tetrazolium, 10 mg β-NADPH, and 0.2% Triton X-100 in 10 mL of 0.05 M Tris buffer for 30 min at 37 °C. The reaction was terminated with 0.05 M Tris buffer washes.

qRT-PCR

Total RNA was extracted from isolated hippocampal tissue using RNeasy mini kit (Qiagen) and treated with deoxyribonuclease 1. For each tissue, 1 μg of total RNA was reverse transcribed using an iScript™ cDNA synthesis kit according to the manufacturer's instructions (BioRad). Real-time PCR reactions were performed using 25–100 ng of template cDNA per reaction and Taqman gene expression 'assay on demand' assays. The target primer/probes used were FAM-labelled *Ncf1* (Mm00447921_m1), *Nfkbia* (Mm00477798_m1), *Nos2* (Mm00440502_m1), *Ppargc1a* (Mm01208835_m1), and *Stip1* (Mm00489584_m1). Reactions were multiplexed and normalised to a VIC-labelled primer/probe for β-actin (Actb; Mm00607939_s1). Relative mRNA expression in each region was determined by normalising to the average amount of hippocampus or cortex from NBH mice using the ΔΔCT method.

Electrophysiology

Brain slices were prepared from animals killed by cervical dislocation. Whole-cell patch recordings were made from visually identified mouse CA1 neurons in acute brain slices (300 μm thick) of the hippocampus as described previously [40, 41]. Patch pipettes were pulled from glass capillaries (GC150F-7.5, o.d. 1.5 mm, Harvard Apparatus, Edenbridge, UK) and had resistances of 3.5–5 MΩ when filled with the pipette solution. Series resistances were between 15 and 20 MΩ (series resistance compensation and prediction were around 70%). Data were recorded using a Multiclamp 700B amplifier (Molecular Devices, Sunnyvale, CA, USA). Stimulation, data acquisition, and analysis were performed using pClamp 10.4 and Clampfit 10.4 (Molecular Devices). An artificial cerebrospinal fluid (aCSF) was used for slice incubation, maintenance after slicing, and perfusion during recordings (125 mM NaCl, 2.5 mM KCl, 26 mM $NaHCO_3$, 10 mM glucose, 1.25 mM NaH_2PO_4, 2 mM sodium pyruvate, 3 mM myo-inositol, 2 mM $CaCl_2$, 1 mM $MgCl_2$, 0.5 mM ascorbic acid, pH 7.4 when gassed with 95% O_2, 5% CO_2). Osmolarity was adjusted to 310 mosmol/l. A low-sodium aCSF was used during preparation of slices, with a composition as above for aCSF, except that NaCl was replaced by 200 mM sucrose, and $CaCl_2$ and $MgCl_2$ were changed to 0.1 mM and 4 mM, respectively. The pipette solution for whole-cell recordings contained 120 mM potassium methanesulfonate or caesium chloride, 10 mM HEPES, 0.2 mM EGTA, 4 mM K-ATP, 0.3 mM Na-GTP, 8 mM NaCl, 10 mM KCl, pH 7.4 with osmolarity between to 280-290 mosmol/l. Synaptic stimulation at the

Schaffer collateral was achieved using an isolated stimulator (Digitimer, Welwyn Garden City, UK; 1–10 V, 0.1–0.2 ms) *via* a bipolar platinum electrode.

Potassium and sodium currents were recorded in CA1 pyramidal neurons by whole-cell voltage clamp, action potentials (AP) in current clamp. Holding potentials were -60 mV and voltage command steps ranged from -110 mV to +50 mV (200 ms) for potassium current measurements and pre-pulse potentials (400 ms) ranged from -110 mV to +50 mV for sodium current recordings. APs were evoked by 50 pA-step current injections ranging from -100 pA to +400 pA.

Cumulative postsynaptic current analysis: The apparent size of the ready releasable pool of vesicles (RRP) was probed by the method of cumulative evoked excitatory postsynaptic current (eEPSC) amplitudes. Stimulus trains (30 Hz for 1 s) were calculated as the difference between peak and baseline before stimulus onset of a given eEPSC. Receptor desensitization was not blocked as it did not affect eEPSC amplitudes, because a comparison of the decay of the first and the last eEPSC within a train did not reveal any significant difference in decay kinetics. The number of release-ready vesicles pool size was obtained by back extrapolating a line fit to the linear phase of the cumulative eEPSC plot to time zero.

Ultrahigh performance liquid chromatography-tandem mass spectroscopy (UPLC–MS/MS)

Mass spectrometry studies were performed by Metabolon. Samples were prepared using the automated MicroLab STAR® system (Hamilton Company). To remove protein, dissociate small molecules bound to protein or trapped in the precipitated protein matrix, and to recover chemically diverse metabolites, proteins were precipitated with methanol under vigorous shaking for 2 min (Glen Mills GenoGrinder 2000) followed by centrifugation. The resulting extract was divided into five fractions: two for analysis by two separate reverse phase (RP)/UPLC-MS/MS methods with positive ion mode electrospray ionization (ESI), one for analysis by RP/UPLC-MS/MS with negative ion mode ESI, one for analysis by HILIC/UPLC-MS/MS with negative ion mode ESI and one sample was reserved for backup. Samples were placed briefly on a TurboVap® (Zymark) to remove the organic solvent. The sample extracts were stored overnight under nitrogen before preparation for analysis. The platform used by Metabolon integrates the chemical analysis, including identification and relative quantification, data reduction, and quality assurance components of the process. Workflow including extraction of raw data, peak-identification, and quality control processed on the assay platform, has been described previously [8].

Statistical analysis

Results are expressed as the means ± S.E.M. Statistical comparisons were made by one-way analysis of variance (ANOVA) with Newman–Keuls posteriori analysis, two-way ANOVA with Bonferroni's multiple comparisons test, Kolmogorov-Smirnov test for non-parametric data distributions or unpaired Student's *t*-test, as appropriate. A *P*-value smaller than 0.05 was considered as significant. All statistical tests were performed using GraphPad Prism v7 software.

Study approval

All animal work conformed to the United Kingdom Home Office regulations. All procedures (both non-regulated and regulated) were conducted under a Home Office project licence awarded to Joern Steinert under the Animals (Scientific Procedures) Act 1986.

Results

Prion diseased mice show signs of neuroinflammation prior to neuronal dysfunction.

Previously we have found that in the hippocampus and cortex of prion infected mice the neuronal metabolism, not only related to the NO signalling cascade, is aberrantly regulated at 10 w.p.i. [8]. At this advanced time point we found evidence for numerous pathological markers such as high levels of misfolded prion protein (PrP^{Sc}) in the hippocampus and cortex, enhanced *glial* fibrillary acidic protein (GFAP) expression associated with nitrergic and oxidative stress, and hippocampal neuronal loss as well as learning and memory deficits [37, 41]. However, as the disease is highly progressed by 10 w.p.i., here we investigated earlier disease-relevant pathways which may enhance a potential rescue of neurodegeneration. We examined the contributions of neuroinflammatory and oxidative stress-related signalling in prion infected mice (RML) at a time point prior to onset of reported disease symptoms (at 6 w.p.i.), as well as advanced stage disease (at 9-10 w.p.i.). We first tested gene expression for the inflammatory suppressor of NF-kB signalling, *Ikba*, and found it to be downregulated at 6 w.p.i. (P=0.038, two-way ANOVA, n=4 mice each, Fig. 1a). RNA expression for the peroxisome proliferator-activated receptor-gamma coactivator, PGC-1α, which controls the expression of genes related to the generation of ROS and prevents oxidative stress by reducing the production of ROS [42], is also downregulated at this early stage of disease (P=0.0015, two-way ANOVA, n=4 mice each, Fig. 1c), as is the prion-interacting protein stress-inducible phosphoprotein 1, STIP1 [43] (P=0.0013, two-way ANOVA, n=4 mice each, Fig. 1d). At 10 w.p.i. we found a strong increase in mRNA levels for *Ikba* (P=0.012) as well as *NCF1* (P<0.0001), one of the components of NADPH oxidase (p47-phox, Fig. 1a, b, n=4 mice each). Furthermore, *PGC-1a* (P<0.0001, two-way ANOVA) and *STIP1* (P=0.0047, two-way ANOVA) mRNA levels remain reduced at this later disease stage (Fig. 1c, d). Importantly, *Nos2* mRNA (iNOS) is increased at 10 w.p.i. (P=0.0266, two-way ANOVA, Fig. 1e) with *Nos1* (nNOS) and *Nos3* (eNOS) mRNA levels being strongly reduced at 6 and 10 w.p.i. (Additional file 1: Figure S1). The enhanced iNOS activity is likely a result of activated astroglia signaling which we further illustrated using the NADPH diaphorase assay at 6-12 w.p.i. (Fig. 1f). We have previously shown that NBH mice lack any significant NADPH diaphorase signals at 10 w.p.i. [8]. This data illustrates a strong increase of NOS (NADPH activity) from 8 w.p.i. onwards in RML mice with signals reminiscent of activated astroglia in the CA1 region spreading to the whole hippocampus at 10 and 12 w.p.i.. Further characteristics for upregulated astroglia were detected by immunostaining for GFAP which showed a significantly stronger expression at 10 w.p.i. in RML hippocampi (P=0.045, Student's *t*-test, Fig. 1g). Altogether our data indicate that an early onset neuroinflammatory contribution to prion disease is detectible from 8 weeks onwards. Thus our approach to start targeting NO signaling will focus on time points following 6 w.p.i. onwards.

Rescue of functional neuronal decline in neurodegeneration by reducing nitrergic stress.

We asked whether interference with neuroinflammatory NO signalling prior to detectable prion misfolding might alleviate some of the neuronal symptoms reported in the disease. In order to address this question, subsequent studies only focussed on RML mice and the effects of treatment since we did not find any indications for aberrant nitrergic signalling in NBH controls (Fig. 1). We quantified the function of CA1 pyramidal neurons and their Schaffer collateral-mediated synaptic inputs as a read-out of neuronal health in RML prion-infected mice treated daily from 6 w.p.i. with the NOS inhibitor, *L-NAME* in comparison to age-matched vehicle RML controls. Both cohorts were assessed by electrophysiology at 7 and 9 w.p.i.. These time points were chosen to study the effects of NOS manipulation based on data presented in Figure 1 at which we expect pathological neuroinflammation to become dominant. Fig. 2a shows representative Schaffer collateral-evoked excitatory postsynaptic currents (eEPSC) in pyramidal CA1 neurons in RML mice at 7 and 9 w.p.i. following stimulation by a 30 Hz train. The recordings illustrate a vast deterioration in neuronal function by 9 w.p.i.. Mean train eEPSC amplitudes from vehicle (RML) or L-NAME treated mice are summarised in Fig. 2b, c (RML, black; +L-NAME, red, n=9 mice each).

Following 3 weeks of daily treatment with L-NAME, mean initial current amplitudes were increased at 9 w.p.i. compared to RML vehicle control mice (P=0.029, two-way ANOVA, Fig. 2d). Cumulative postsynaptic current analysis (Fig. 2e, f), a measure to estimate available vesicle pool sizes based on the cumulative eEPSC amplitude plots, revealed a strong recovery of the vesicular pool size at 9 w.p.i. following L-NAME treatment (P=0.043, two-way ANOVA, Fig. 2g) suggesting an improvement of synapse function. An important regulatory mechanism for synaptic release is the control of release probabilities. As a measure to determine the initial synaptic release probabilities we assessed paired-pulse ratios (PPR, $eEPSC_2/eEPSC_1$ amplitudes) at 33 ms inter-spike intervals of Schaffer collateral-stimulated eEPSCs in diseased and treated mice. PPR values of synaptic responses in hippocampi from diseased mice revealed a significant increase at 9 w.p.i. indicating a reduction in release probability over time (P=0.0145, two-way ANOVA, Fig. 2h). L-NAME treatment, however, suppressed this increase in PPRs, which suggests that NOS inhibition prevents different aspects of synapse dysfunction (Fig. 2h). A further assessment criterion of neuronal health is the ability of synapses to spontaneously release vesicles. These spontaneous or miniature EPSCs (mEPSC) provide important signals for physiological neuronal homeostatic signaling [44]. Consistent with a general neuronal dysfunction in prion disease, we found that miniature EPSC (mEPSC) amplitudes and spontaneous firing frequencies were reduced at 9 w.p.i. (Fig. 3a-c). Analyzing the relative cumulative distributions of mEPSC amplitudes and inter-spike-intervals (ISI) revealed a strong leftward shift in amplitudes and rightward shift in ISI in prion disease at 9 w.p.i. compared to 6 w.p.i. (Fig. 3b, c, amplitudes: P<0.0001, D=0.571; ISI: P<0.0001, D=0.738, Kolmogorov-Smirnov test: 9 vs 6 w.p.i.) confirming again compromised neurotransmission. A protective effect of L-NAME treatment was observed at 9 w.p.i. (Fig. 3b, c, amplitudes: P<0.0001, D=0.571; ISI: P<0.0001, D=0.683, Kolmogorov-Smirnov test: 9 w.p.i. vs 9 w.p.i. + L-NAME treatment). The effects of prion disease are further illustrated for mean mEPSC amplitudes and frequencies (Fig. 3d, e, black, P<0.05, one-way ANOVA) and importantly, L-NAME treatment leads to recovery of both parameters over the time course of the disease (Fig. 3d, e, red, P<0.05, one-way ANOVA).

We also assessed neuronal function by measuring the ability of CA1 pyramidal neurons to generate current-evoked action potentials (AP), and characterized the underlying whole-cell potassium and sodium currents. Both, the ion channel functions and AP propagation play crucial roles in regulating neuronal performance and allow the neurons to sustain information transmission. AP parameters such as half width and amplitude are main characteristics, both predominately determined by potassium and sodium channel activities, respectively. L-NAME treatment led to a reduction of the increased AP half-width at 9 w.p.i. indicating an augmentation of potassium currents (P=0.002, one-way ANOVA). AP amplitudes were reduced at 7 w.p.i. (P=0.271, one-way ANOVA) and increased at 9 w.p.i. (P=0.018, one-way ANOVA) following L-NAME treatment (Fig. 4a, b). As both measures are determined by the activities of voltage-gated potassium and sodium channels, we directly assessed both, potassium and sodium currents by voltage-clamp. Current-Voltage (IV) relationships show a strong decline of outward potassium currents (Fig. 4c, d) and inward sodium currents (Fig. 4e) at 9 w.p.i. confirming the observed changes in AP parameters, with L-NAME treatment recovering both currents substantially at 9 w.p.i., substantiating the AP data at 9 w.p.i. and confirming a neuroprotective role of L-NAME treatment. The data on neuronal physiology were supported by measurements of levels of neuronal protein involved in synaptic function and neuronal fidelity. Protein levels of several synaptic markers, including MUNC 18, SNAP-25 and complexin 1/2 were reduced with others showing strong tendencies of lower expression (synaptophysin, synaptobrevin, synapsin) at 9 w.p.i. (Additional file 2: Figure S2). Protein expression of the voltage-gated potassium channel Kv3.1, the main conductance contributing to the IV relationships in Fig. 4c, d and determinant of AP half width, shows a decline at 9 w.p.i.. Altogether, the data illustrate the broad neuronal dysfunction at later disease stages and the potent effects of L-NAME treatment to recover several aspects of neuronal dysfunction by suppressing excessive NO signaling *in vivo*.

Protein 3-nitrotyrosination is driven by oxidative stress and enhances protein glycation in prion disease.

Protein 3-nitrotyrosination is characteristic of protein-misfolding neurodegeneration [22, 45]. 3-NT occurs under conditions of oxidative stress and aberrant nitrergic activity. We confirmed a decreased ratio of reduced to oxidized glutathione GSH/GSSG in prion diseased mice at 9 w.p.i. (P=0.0039, control NBH *vs* RML mice, Student's *t*-test, Fig. 5a) providing evidence for enhanced oxidative stress as one hallmark of the disease and confirming previously reported increases in oxidative stress levels in prion-diseased mice [8]. Together with the enhanced levels of nitrergic stress associated with augmented expression levels of iNOS mRNA (Fig. 1), we found total amounts of 3-nitrotyrosinated proteins to be >5-fold elevated in prion infected mice compared to NBH controls at 9 w.p.i. (P=0.0005, control NBH vs RML, one-way ANOVA, Fig. 5b). Importantly, following treatment with the NOS inhibitor L-NAME, these elevated levels of 3-NT could be reversed back to control values (P=0.0005, RML+L-NAME vs RML, one-way ANOVA, Fig. 5b).

Both AD and CJD are associated with neurotoxic glycation signalling as well as a strong presence of AGEs [22, 23, 36]. AGEs are produced by the non-enzymatic glycation of amino compounds with reducing sugars through a series of sequential and irreversible reactions. The predominant neuronal precursor to induce protein glycation is DHAP which spontaneously forms methylglyoxal, a strong glycating agent [46]. We have measured DHAP by mass spectrometry and found levels to be ~2-fold increased (P=0.0027,

Student's *t*-test, Fig. 5c) in the hippocampus of prion-infected mice. As TPI is the upstream enzyme in the cascade to produce DHAP, a reduction of its enzymatic activity would be responsible for the observed changes in the levels of its metabolites. It has been previously reported that mutations of TPI carrying the tyrosine substitutions Y165F and Y209F, both of which are located at the catalytic center, render this enzyme inefficient when expressed in human neuroblastoma cells thereby shifting the balance between GAP and DHAP towards the latter and reducing cell viability [23]. Based on these findings, we tested whether we could detect a nitrergic post-translational modification of TPI in prion-diseased mice that would ultimately be responsible for an accumulation of DHAP. Indeed, when performing immunoblotting for 3-nitrotyrosination after having immuno-precipitated TPI, we detected an increase of 3-NT TPI protein levels in disease (P=0.033, one-way ANOVA, RML vs NBH, Fig. 5d). Importantly, treatment with L-NAME prevented the increase in 3-NT TPI levels and reversed it back to control levels (P=0.484, one-way ANOVA, NBH vs RML+L-NAME, Fig. 5d). Total amounts of TPI protein were unchanged (P=0.163, one-way ANOVA, Fig. 5f). The production of AGE following TPI nitrotyrosination is directly linked to the activation of the receptor for AGE (RAGE) and the expression of RAGE reflects a positive confirmation for AGE signaling [47]. To test whether we could confirm AGE signaling in prion mice we examined RAGE expression and found that prion diseased mice exhibited markedly enhanced levels of RAGE (P=0.0074, one-way ANOVA, Fig. 5e). We tested the effects of NOS inhibition on RAGE expression and found that treatment with L-NAME ameliorated these increases (P=0.0243, one-way ANOVA, Fig. 5e, note the lower band represents actin) providing strong evidence for the NO-mediated 3-NT/TPI/DHAP/RAGE signaling cascade in prion disease which signifies a disease-associated neurotoxic pathway.

Nitric oxide and glycation signalling impact on prion misfolding.

The pathological scrapie form of the prion protein is heavily glycated resulting in mainly N^{ε}-(carboxymethyl)lysines at up to eight lysine residues, whereas PrP^{C} does not contain glycated amino acids [48, 49]. It has been shown that mono- or di-glycation affects the molecular weight of the prion protein resulting in multiple bands following immunoblotting. We thus tested for expression of prion protein in hippocampal tissues. Importantly, we noticed the occurrence of bands above the expected PrP^{c} molecular weight (~36 kDa) in hippocampal samples of RML mice at 9 w.p.i. detected using the ICSM35 antibody raised to specifically recognise β-sheet-rich structures within prion proteins [50, 51] (Fig. 6a). These higher weight bands might therefore reflect glycated and β-sheet-enriched prion protein.

We next assessed hippocampal tissue by immunocytochemistry and stained for prion protein to investigate the localisation of the misfolded protein in NBH and RML mice with and without L-NAME treatment. In order to specifically visualise β-sheet-rich PrP^{Sc} that is prerequisite for prion aggregation we immunostained samples using the ICSM35 antibody [50, 51]. We found that prion signals were almost exclusively detected in the cytosol of cubiculum neurons in RML mice reminiscent of possible protein aggregates formed within the cytosol [49, 52] (Fig 6b, c). Cubiculum areas from NBH mice did not show any labelling in neurons (Fig. 6b) confirming PrP^{Sc} specific detection in RML mice (note also the strong loss of DAPI signals in RML samples indicative of substantial neuronal loss which was reversed after L-

NAME treatment, Fig. 6b). Following counting of ICSM35-positive (PrP^{Sc}) cells in the hippocampus, we found larger proportions of cells in RML mice compared to RML mice receiving L-NAME treatment suggesting a reduction in the occurrence of prion protein misfolding (RML: 38.8 ± 4.1%, RML+L-NAME: 23.4 ± 2.7%, total cell number: 679, P=0.0346, Student's *t*-test, [n=5 RML mice, n=3 RML+L-NAME treated mice], Fig. 6b, c). These data therefore indicate that reducing nitrergic stress could slow down the progression of protein misfolding and/or aggregation. We further noticed that the absolute numbers of pyramidal neurons in the hippocampus of L-NAME treated mice was similar from control NBH hippocampi whereas vehicle treated RML mice showed a significant reduction in cell numbers (NeuN positive cells per mm^2: NBH: 0.0021 ± 0.0001 (n=3 mice); RML: 0.0007 ± 0.0001 (n=5 mice), P=0.0324 vs NBH; RML+L-NAME: 0.0013 ± 0.0003 (n=3 mice), one-way ANOVA; Fig. 6b, d (representative images of NeuN and DAPI labelled tissues). This data suggest that L-NAME treatment results in a reduction of neuronal loss consistent with the L-NAME mediated rescue of neuronal function at this time point of disease (Fig. 2-4).

Previously we reported that the metabolome of the hippocampus as well as the cortex is altered in prion disease, with both regions showing significant increases in nitrergic and oxidative stress signalling at 10 w.p.i. [8]. Furthermore, diseased mice exhibit behavioural deficiencies in burrowing activity at 9 w.p.i. [37], a behaviour associated with hippocampal but also cortical dysfunction [53]. In parallel to the hippocampal increases in DHAP levels, we also confirmed enhanced levels of DHAP in the cortex of RML mice (scaled intensity: NBH: 0.81 ± 0.07, n=8; RML: 1.07 ± 0.07, n=8; P=0.023, Student's *t*-test, data not shown) suggesting a similar upregulated glycation signaling which could underlie the observed prion misfolding. To test if we can detect potential signs of prion misfolding in the cortex as well and beneficial effects of L-NAME treatment in cortical regions at 9 w.p.i. we assessed cortical tissues for misfolded prion protein by immunocytochemistry. We found that in the cortex from RML mice prion protein positive signals exhibit clusters within the cytosol showing typical punctate form of localisation pattern as seen in the immunocytochemistry data in the hippocampus reflecting misfolding of the protein which was absent in tissue from NBH mice (Additional file 3: Figure S3a). Following counting of cells exhibiting such PrP^{Sc} clusters, we found that RML samples exhibited high numbers which were greatly reduced following L-NAME treatment suggesting a reduction of neurons possessing b-sheet-rich prion protein (RML: 95.0 ± 2.2%, RML+L-NAME: 24.2 ± 5.1%, total cell number: 1892, P<0.0001, Student's *t*-test, [n=5 RML mice, n=3 RML+L-NAME treated mice], Additional file 3: Figure S3b). Importantly, we also assessed the total number of cortical neurons and found that L-NAME treatment reversed the reduction in cell loss caused by disease (cells per mm^2: NBH: 0.0022 ± 0.0002 (n=3 mice); RML: 0.0014 ± 0.00006 (n=5 mice), P=0.0119 vs NBH; RML+L-NAME: 0.0018 ± 0.00004 (n=3 mice), one-way ANOVA; Additional file 3: Figure S3a, c).

Together, our data provide evidence that *in vivo* NOS inhibition for 3 weeks can reduce the amount of prion protein misfolding which positively impacts on neuronal health. We propose that nitrergic stress exerts its effects *via* post-translational modification, and associated inhibition, of TPI leading to an accumulation of glycated proteins. The resulting generation of advanced glycation end products may

impact on prion protein misfolding as AGE-assisted conversion of PrP^{C} into PrP^{Sc} itself as it is reported for α-synuclein [26, 27] or Ab [31].

Discussion

This study was set out to investigate the role of nitrergic stress in the development of protein misfolding neuropathology using prion-mediated neurodegeneration as a well-established disease system. We show that prion disease is characterised by a range of dysfunctional pathways involving oxidative stress and neuroinflammatory nitrergic signalling as well as activation of the glycation-AGE signalling cascade. Importantly, we also show that diminishing cytotoxic NO levels throughout early disease stages can reduce the progression of the neuronal pathology as revealed by sustained synaptic and neuronal function, the associated suppression of glycation signalling and the reduced generation of misfolded prion protein in the hippocampus and cortex of infected animals. Although NO signalling plays an important role in physiological neuronal function including regulation of ion channel activities [40, 54, 55] or several aspects of neurotransmission [56, 57], NO dysregulation and nitrergic stress have long been associated with numerous neurodegenerative diseases [3, 9, 19, 58, 59]. Its main disease-relevant neurotoxic signaling involves post-translational protein modifications, such as S-nitrosylation and 3-nitrotyrosination. For instance, it has been shown in various systems that S-nitrosylation of synaptic proteins such as AMPA receptors [60], syntaxin [61], complexin [62], stargazin [63, 64] or dynamin [65] can modify their functions (for review [4]). Several studies have confirmed that supressing excess NO production might be beneficial under various conditions of neuroinflammation which is a major hallmark of protein misfolding diseases. As such targeting NO signalling and NO-mediated post-translational modifications presents an attractive target for treatment in neuropathology [9]. For instance, a potent iNOS inhibitor, GW274150, has been used in Phase II clinical trials to treat migraine and other NOS inhibitors are known to provide neuroprotection in PD [13] or under conditions of cerebral ischemia and cerebral artery occlusions [66, 67]. In various models of neurodegeneration pharmacological inhibition of iNOS produced beneficial effects [14, 15] confirming that blocking nitrergic neurotoxicity can protect the central nervous system [68]. In addition, two NOS blockers, L-NNA and L-NAME, have been used in human trials to treat septic shock, although with mixed outcome, this requires further investigations (for review see [69]).

However, the exact downstream targets of NO and signaling routes in disease remain elusive despite the identification of numerous modified proteins. However, there is growing evidence that high nitrergic activity in conjunction with enhanced oxidative stress can directly result in activation of a cascade involving glycation signalling [20, 70-72], presenting a positive feedback loop to promote cell death. Furthermore, nitrergic and oxidative stress facilitates the formation of peroxynitrite, which in turn, leads to 3-nitrotyrosination of cellular proteins. For example, 3-NT formation of Aβ at tyrosine 10 promotes its aggregation [12, 19] thereby increasing its synaptotoxicity. Glycation has been detected in AD and CJD in earlier studies [35, 73, 74], however, disease-related 3-NT signalling has only recently been proposed to involve glycation signalling in AD [21]. This specific pathway requires the dysregulation of glycolysis *via*

the 3-NT-mediated suppression of triose phosphate isomerase activity which results in increased cellular levels of DHAP. DHAP spontaneously decomposes to methylglyoxal, which is a highly reactive a-oxo-aldehyde that can modify both, proteins and DNA to form AGEs. Methylglyoxal can be metabolised by the glyoxalase pathway, which requires the presence of GSH (summary pathway, Fig. 7). As our data show reductions in neuronal GSH levels and associated enhanced oxidative stress levels in prion disease [8], it suggests that this detoxifying pathway might also be compromised. The downstream consequences of increased AGE levels are not fully understood but emerging evidence suggests that this irreversible modification renders many proteins inactive and susceptible to misfolding such as in the case of α-synuclein [26, 27] or Ab [31] or further increases oxidative stress due to super oxide dismutase inhibition [75]. In our study, we could show that pharmacological suppression of NO signalling, predominantly targeting neuroinflammatory iNOS generated NO, leads to diminished 3-NT of TPI and subsequent reduction of AGE formation, as detected by reduced RAGE expression. These effects are associated with diminished levels of misfolded prion protein (PrP^{Sc}) and improved neuronal health as measured electrophysiologically and confirmed by higher numbers of pyramidal neurons in the hippocampus and cortex of treated animals. Since one mechanism that leads to the stabilisation and deposition of PrP^{Sc} fibrils may be the result of specific AGE modifications of PrP^{Sc}, it is possible that inhibition of NO-mediated AGE formation, as demonstrated here, might be an approach of slowing PrP^{Sc} misfolding, thereby alleviating the progression of prion disease.

Conclusions

The established correlation between protein glycation – as reported for several misfolding proteins – and prion misfolding might link the NO signalling cascade to the neuroprotective effect seen following treatment with L-NAME. Together, we present new evidence for the link between NO-mediated post-translational modifications of an enzyme directly connecting NO and glycation signalling. We postulate that the pharmacologically abolished AGE formation, *via* NOS inhibition, positively impacts on prion protein misfolding thereby slowing or reducing prion aggregation. This could present an approach to diminish the detrimental neuroinflammatory effect seen in neurodegeneration [76] since our evidence of prolonged neuronal health as a result of treatment implicates this signalling route as an important contributor to neuronal degeneration (Fig. 7) and highlights nitrergic stress and glycation signalling as a putative target for disease-modifying treatments. To take this study forward it will be important to further dissect the NO-mediated identities of AGEs and downstream RAGE signalling, with particular interest in the positive feedback loop of AGE-formation of misfolding proteins and the pro-neuroinflammatory contributions of RAGE signaling.

Abbreviations

3-NT: 3-nitrotyrosine

AGE: advanced glycation end products

AD: Alzheimer’s disease

CJD: Creutzfeldt Jakob Disease

DHAP: dihydroxyacetone phosphate

eEPSC: evoked excitatory postsynaptic current

eNOS: endothelial NOS

GAP: glyceraldehyde 3-phosphate

GFAP: *glial* fibrillary acidic protein

HC: hippocampus

HPLC: high-performance liquid chromatography

iNOS: inducible NOS

ISI: inter-spike-intervals

i.p.: Intraperitoneal

L-NAME: N(ω)-nitro-L-arginine methyl ester

L-NOARG: L-NG-nitro arginine

LC/MS: Liquid chromatography–mass spectrometry

mEPSC: miniature EPSC

nNOS: neuronal NOS

NO: nitric oxide

NOS: NO synthase

NBH: normal brain homogenate

PD: Parkinson’s disease

PrP^{Sc}: misfolded prion protein

PBS: Phosphate-buffered saline

PPR: paired-pulse ratios

RAGE: receptor for AGE

RML: Rocky Mountain Laboratory

RRP: releasable pool of vesicles

ROS: reactive oxygen species

TPI: triose-phosphate isomerase

w.p.i.: weeks post inoculation

Declarations

Ethics approval and consent to participate

All animal work conformed to the United Kingdom Home Office regulations. All procedures (both non-regulated and regulated) were conducted under a Home Office project licence awarded to Joern Steinert under the Animals (Scientific Procedures) Act 1986.

Consent for publication

Not applicable

Availability of data and materials

All data generated or analysed during this study are included in this published article [and its supplementary information files].

Competing interests

The authors declare no conflict of interest.

Author contributions

JMB and JRS designed research; JMB, SWR, JGS, HS and CO performed studies, SJB and ABT contributed with analytical tools and had intellectual input. JMP, JRS and JGS wrote the paper with inputs from SJB and ABT. All authors read and approved the final manuscript.

Funding

This work was supported by The Henry Smith Charity, UK (JMB), the Medical Research Council, UK (JRS, SWR, JGS, HS, SJB, ABT) and University of Nottingham (CO).

Acknowledgements

We thank Prof F. Giorgini (University of Leicester, UK) for helpful discussions in preparation of this manuscript.

References

1. Brosseron F, Kolbe CC, Santarelli F, Carvalho S, Antonell A, Castro-Gomez S, et al. Multicenter Alzheimer's and Parkinson's disease immune biomarker verification study. Alzheimers Dement. 2020;16(2):292-304.
2. Zou C, Shi Y, Ohli J, Schuller U, Dorostkar MM, Herms J. Neuroinflammation impairs adaptive structural plasticity of dendritic spines in a preclinical model of Alzheimer's disease. Acta Neuropathol. 2016;131(2):235-46.
3. Steinert JR, Chernova T, Forsythe ID. Nitric Oxide Signaling in Brain Function, Dysfunction, and Dementia. Neuroscientist. 2010;16(4):435-52.
4. Bradley SA, Steinert JR. Nitric Oxide-Mediated Posttranslational Modifications: Impacts at the Synapse. Oxid Med Cell Longev. 2016;2016:5681036.
5. Sbodio JI, Snyder SH, Paul BD. Redox Mechanisms in Neurodegeneration: From Disease Outcomes to Therapeutic Opportunities. Antioxid Redox Signal. 2019;30(11):1450-99.
6. Nakamura T, Prikhodko OA, Pirie E, Nagar S, Akhtar MW, Oh CK, et al. Aberrant protein S-nitrosylation contributes to the pathophysiology of neurodegenerative diseases. Neurobiol Dis. 2015;84:99-108.
7. Chen LN, Sun J, Yang XD, Xiao K, Lv Y, Zhang BY, et al. The Brain NO Levels and NOS Activities Ascended in the Early and Middle Stages and Descended in the Terminal Stage in Scrapie-Infected Animal Models. Mol Neurobiol. 2017;54(3):1786-96.
8. Bourgognon JM, Spiers JG, Scheiblich H, Antonov A, Bradley SJ, Tobin AB, et al. Alterations in neuronal metabolism contribute to the pathogenesis of prion disease. Cell Death Differ. 2018;25(8):1408-25.
9. Nakamura T, Lipton SA. Protein S-Nitrosylation as a Therapeutic Target for Neurodegenerative Diseases. Trends Pharmacol Sci. 2016;37(1):73-84.
10. Nakamura T, Lipton SA. Redox modulation by S-nitrosylation contributes to protein misfolding, mitochondrial dynamics, and neuronal synaptic damage in neurodegenerative diseases. Cell Death Differ. 2011;18(9):1478-86.
11. Wijasa TS, Sylvester M, Brocke-Ahmadinejad N, Schwartz S, Santarelli F, Gieselmann V, et al. Quantitative proteomics of synaptosome S-nitrosylation in Alzheimer's disease. J Neurochem. 2019.
12. Guivernau B, Bonet J, Valls-Comamala V, Bosch-Morato M, Godoy JA, Inestrosa NC, et al. Amyloid-beta Peptide Nitrotyrosination Stabilizes Oligomers and Enhances NMDAR-Mediated Toxicity. J Neurosci. 2016;36(46):11693-703.
13. Broom L, Marinova-Mutafchieva L, Sadeghian M, Davis JB, Medhurst AD, Dexter DT. Neuroprotection by the selective iNOS inhibitor GW274150 in a model of Parkinson disease. Free Radic Biol Med. 2011;50(5):633-40.

14. Neufeld AH, Sawada A, Becker B. Inhibition of nitric-oxide synthase 2 by aminoguanidine provides neuroprotection of retinal ganglion cells in a rat model of chronic glaucoma. Proc Natl Acad Sci U S A. 1999;96(17):9944-8.
15. Sil S, Ghosh T, Ghosh R, Gupta P. Nitric oxide synthase inhibitor, aminoguanidine reduces intracerebroventricular colchicine induced neurodegeneration, memory impairments and changes of systemic immune responses in rats. J Neuroimmunol. 2016.
16. Spiers JG, Chen HC, Bourgognon JM, Steinert JR. Dysregulation of stress systems and nitric oxide signaling underlies neuronal dysfunction in Alzheimer's disease. Free Radic Biol Med. 2019;134:468-83.
17. Paul BD, Snyder SH. Impaired Redox Signaling in Huntington's Disease: Therapeutic Implications. Front Mol Neurosci. 2019;12:68.
18. Gonzalez-Reyes RE, Nava-Mesa MO, Vargas-Sanchez K, Ariza-Salamanca D, Mora-Munoz L. Involvement of Astrocytes in Alzheimer's Disease from a Neuroinflammatory and Oxidative Stress Perspective. Front Mol Neurosci. 2017;10:427.
19. Kummer MP, Hermes M, Delekarte A, Hammerschmidt T, Kumar S, Terwel D, et al. Nitration of tyrosine 10 critically enhances amyloid beta aggregation and plaque formation. Neuron. 2011;71(5):833-44.
20. Ill-Raga G, Ramos-Fernandez E, Guix FX, Tajes M, Bosch-Morato M, Palomer E, et al. Amyloid-beta peptide fibrils induce nitro-oxidative stress in neuronal cells. J Alzheimers Dis. 2010;22(2):641-52.
21. Guix FX, Ill-Raga G, Bravo R, Nakaya T, de Fabritiis G, Coma M, et al. Amyloid-dependent triosephosphate isomerase nitrotyrosination induces glycation and tau fibrillation. Brain. 2009;132(Pt 5):1335-45.
22. Tajes M, Eraso-Pichot A, Rubio-Moscardo F, Guivernau B, Ramos-Fernandez E, Bosch-Morato M, et al. Methylglyoxal produced by amyloid-beta peptide-induced nitrotyrosination of triosephosphate isomerase triggers neuronal death in Alzheimer's disease. J Alzheimers Dis. 2014;41(1):273-88.
23. Tajes M, Eraso-Pichot A, Rubio-Moscardo F, Guivernau B, Bosch-Morato M, Valls-Comamala V, et al. Methylglyoxal reduces mitochondrial potential and activates Bax and caspase-3 in neurons: Implications for Alzheimer's disease. Neurosci Lett. 2014;580:78-82.
24. Lapolla A, Traldi P, Fedele D. Importance of measuring products of non-enzymatic glycation of proteins. Clinical Biochemistry. 2005;38(2):103-15.
25. Miranda HV, Outeiro TF. The sour side of neurodegenerative disorders: the effects of protein glycation. The Journal of Pathology. 2010;221(1):13-25.
26. Vicente Miranda H, Szego EM, Oliveira LMA, Breda C, Darendelioglu E, de Oliveira RM, et al. Glycation potentiates alpha-synuclein-associated neurodegeneration in synucleinopathies. Brain. 2017;140(5):1399-419.
27. Vicente Miranda H, Gomes MA, Branco-Santos J, Breda C, Lazaro DF, Lopes LV, et al. Glycation potentiates neurodegeneration in models of Huntington's disease. Sci Rep. 2016;6:36798.
28. Castellani RJ, Harris PL, Sayre LM, Fujii J, Taniguchi N, Vitek MP, et al. Active glycation in neurofibrillary pathology of Alzheimer disease: N(epsilon)-(carboxymethyl) lysine and hexitol-lysine.

Free Radic Biol Med. 2001;31(2):175-80.

29. Yan SD, Chen X, Schmidt AM, Brett J, Godman G, Zou YS, et al. Glycated tau protein in Alzheimer disease: a mechanism for induction of oxidant stress. Proc Natl Acad Sci U S A. 1994;91(16):7787-91.
30. Münch G, Mayer S, Michaelis J, Hipkiss AR, Riederer P, Müller R, et al. Influence of advanced glycation end-products and AGE-inhibitors on nucleation-dependent polymerization of β-amyloid peptide. Biochimica et Biophysica Acta (BBA) - Molecular Basis of Disease. 1997;1360(1):17-29.
31. Ng J, Kaur H, Collier T, Chang K, Brooks AES, Allison JR, et al. Site-specific glycation of Abeta1-42 affects fibril formation and is neurotoxic. J Biol Chem. 2019;294(22):8806-18.
32. Emendato A, Milordini G, Zacco E, Sicorello A, Dal Piaz F, Guerrini R, et al. Glycation affects fibril formation of Abeta peptides. J Biol Chem. 2018;293(34):13100-11.
33. Chavakis T, Bierhaus A, Nawroth PP. RAGE (receptor for advanced glycation end products): a central player in the inflammatory response. Microbes and Infection. 2004;6(13):1219-25.
34. Higai K, Shimamura A, Matsumoto K. Amadori-modified glycated albumin predominantly induces E-selectin expression on human umbilical vein endothelial cells through NADPH oxidase activation. Clinica Chimica Acta. 2006;367(1):137-43.
35. Andreoletti O, Levavasseur E, Uro-Coste E, Tabouret G, Sarradin P, Delisle MB, et al. Astrocytes accumulate 4-hydroxynonenal adducts in murine scrapie and human Creutzfeldt-Jakob disease. Neurobiol Dis. 2002;11(3):386-93.
36. Freixes M, Rodriguez A, Dalfo E, Ferrer I. Oxidation, glycoxidation, lipoxidation, nitration, and responses to oxidative stress in the cerebral cortex in Creutzfeldt-Jakob disease. Neurobiol Aging. 2006;27(12):1807-15.
37. Moreno JA, Radford H, Peretti D, Steinert JR, Verity N, Martin MG, et al. Sustained translational repression by eIF2alpha-P mediates prion neurodegeneration. Nature. 2012;485(7399):507-11.
38. Tracey WR, Tse J, Carter G. Lipopolysaccharide-induced changes in plasma nitrite and nitrate concentrations in rats and mice: pharmacological evaluation of nitric oxide synthase inhibitors. J Pharmacol Exp Ther. 1995;272(3):1011-5.
39. Avontuur JA, Buijk SL, Bruining HA. Distribution and metabolism of N(G)-nitro-L-arginine methyl ester in patients with septic shock. Eur J Clin Pharmacol. 1998;54(8):627-31.
40. Steinert JR, Robinson SW, Tong H, Haustein MD, Kopp-Scheinpflug C, Forsythe ID. Nitric oxide is an activity-dependent regulator of target neuron intrinsic excitability. Neuron. 2011;71(2):291-305.
41. Bradley SJ, Bourgognon JM, Sanger HE, Verity N, Mogg AJ, White DJ, et al. M1 muscarinic allosteric modulators slow prion neurodegeneration and restore memory loss. J Clin Invest. 2017;127(2):487-99.
42. Sahin E, Colla S, Liesa M, Moslehi J, Muller FL, Guo M, et al. Telomere dysfunction induces metabolic and mitochondrial compromise. Nature. 2011;470(7334):359-65.

43. Maciejewski A, Ostapchenko VG, Beraldo FH, Prado VF, Prado MA, Choy WY. Domains of STIP1 responsible for regulating PrPC-dependent amyloid-beta oligomer toxicity. Biochem J. 2016;473(14):2119-30.
44. Hanson MG, Landmesser LT. Normal patterns of spontaneous activity are required for correct motor axon guidance and the expression of specific guidance molecules. Neuron. 2004;43(5):687-701.
45. Knott AB, Bossy-Wetzel E. Nitric oxide in health and disease of the nervous system. Antioxid Redox Signal. 2009;11(3):541-54.
46. Allaman I, Belanger M, Magistretti PJ. Methylglyoxal, the dark side of glycolysis. Front Neurosci. 2015;9:23.
47. Srikanth V, Maczurek A, Phan T, Steele M, Westcott B, Juskiw D, et al. Advanced glycation endproducts and their receptor RAGE in Alzheimer's disease. Neurobiol Aging. 2011;32(5):763-77.
48. Choi YG, Kim JI, Jeon YC, Park SJ, Choi EK, Rubenstein R, et al. Nonenzymatic glycation at the N terminus of pathogenic prion protein in transmissible spongiform encephalopathies. J Biol Chem. 2004;279(29):30402-9.
49. Choi YG, Shin HY, Kim JI, Choi EK, Carp RI, Kim YS. N(epsilon)-Carboxymethyl Modification of Lysine Residues in Pathogenic Prion Isoforms. Mol Neurobiol. 2016;53(5):3102-12.
50. Freir DB, Nicoll AJ, Klyubin I, Panico S, Mc Donald JM, Risse E, et al. Interaction between prion protein and toxic amyloid beta assemblies can be therapeutically targeted at multiple sites. Nat Commun. 2011;2:336.
51. Wenborn A, Terry C, Gros N, Joiner S, D'Castro L, Panico S, et al. A novel and rapid method for obtaining high titre intact prion strains from mammalian brain. Sci Rep. 2015;5:10062.
52. Veith NM, Plattner H, Stuermer CA, Schulz-Schaeffer WJ, Burkle A. Immunolocalisation of PrPSc in scrapie-infected N2a mouse neuroblastoma cells by light and electron microscopy. Eur J Cell Biol. 2009;88(1):45-63.
53. Deacon RM. Burrowing in rodents: a sensitive method for detecting behavioral dysfunction. Nat Protoc. 2006;1(1):118-21.
54. Tozer AJ, Forsythe ID, Steinert JR. Nitric oxide signalling augments neuronal voltage-gated L-type (Ca(v)1) and P/q-type (Ca(v)2.1) channels in the mouse medial nucleus of the trapezoid body. PLoS One. 2012;7(2):e32256.
55. Steinert JR, Kopp-Scheinpflug C, Baker C, Challiss RA, Mistry R, Haustein MD, et al. Nitric oxide is a volume transmitter regulating postsynaptic excitability at a glutamatergic synapse. Neuron. 2008;60(4):642-56.
56. Pigott BM, Garthwaite J. Nitric Oxide Is Required for L-Type Ca(2+) Channel-Dependent Long-Term Potentiation in the Hippocampus. Front Synaptic Neurosci. 2016;8:17.
57. Hardingham N, Dachtler J, Fox K. The role of nitric oxide in pre-synaptic plasticity and homeostasis. Front Cell Neurosci. 2013;7:190.

58. Morris G, Berk M, Klein H, Walder K, Galecki P, Maes M. Nitrosative Stress, Hypernitrosylation, and Autoimmune Responses to Nitrosylated Proteins: New Pathways in Neuroprogressive Disorders Including Depression and Chronic Fatigue Syndrome. Mol Neurobiol. 2017;54(6):4271-91.
59. Zhao Y, Vanhoutte PM, Leung SW. Vascular nitric oxide: Beyond eNOS. J Pharmacol Sci. 2015;129(2):83-94.
60. Selvakumar B, Jenkins MA, Hussain NK, Huganir RL, Traynelis SF, Snyder SH. S-nitrosylation of AMPA receptor GluA1 regulates phosphorylation, single-channel conductance, and endocytosis. Proc Natl Acad Sci U S A. 2013;110(3):1077-82.
61. Palmer ZJ, Duncan RR, Johnson JR, Lian LY, Mello LV, Booth D, et al. S-nitrosylation of syntaxin 1 at Cys(145) is a regulatory switch controlling Munc18-1 binding. Biochem J. 2008;413(3):479-91.
62. Robinson SW, Bourgognon JM, Spiers JG, Breda C, Campesan S, Butcher A, et al. Nitric oxide-mediated posttranslational modifications control neurotransmitter release by modulating complexin farnesylation and enhancing its clamping ability. PLoS Biol. 2018;16(4):e2003611.
63. Selvakumar B, Campbell PW, Milovanovic M, Park DJ, West AR, Snyder SH, et al. AMPA receptor upregulation in the nucleus accumbens shell of cocaine-sensitized rats depends upon S-nitrosylation of stargazin. Neuropharmacology. 2014;77:28-38.
64. Selvakumar B, Huganir RL, Snyder SH. S-nitrosylation of stargazin regulates surface expression of AMPA-glutamate neurotransmitter receptors. Proc Natl Acad Sci U S A. 2009;106(38):16440-5.
65. Wang Z, Kim JI, Frilot N, Daaka Y. Dynamin2 S-nitrosylation regulates adenovirus type 5 infection of epithelial cells. J Gen Virol. 2012;93(Pt 10):2109-17.
66. Nogawa S, Forster C, Zhang F, Nagayama M, Ross ME, Iadecola C. Interaction between inducible nitric oxide synthase and cyclooxygenase-2 after cerebral ischemia. Proc Natl Acad Sci U S A. 1998;95(18):10966-71.
67. Mukherjee P, Cinelli MA, Kang S, Silverman RB. Development of nitric oxide synthase inhibitors for neurodegeneration and neuropathic pain. Chem Soc Rev. 2014;43(19):6814-38.
68. Dawson VL, Dawson TM. Nitric oxide in neuronal degeneration. Proc Soc Exp Biol Med. 1996;211(1):33-40.
69. Vitecek J, Lojek A, Valacchi G, Kubala L. Arginine-based inhibitors of nitric oxide synthase: therapeutic potential and challenges. Mediators Inflamm. 2012;2012:318087.
70. El-Bassossy HM, Neamatallah T, Balamash KS, Abushareb AT, Watson ML. Arginase overexpression and NADPH oxidase stimulation underlie impaired vasodilation induced by advanced glycation end products. Biochem Biophys Res Commun. 2018;499(4):992-7.
71. Greco R, Demartini C, Zanaboni AM, Blandini F, Amantea D, Tassorelli C. Modulation of cerebral RAGE expression following nitric oxide synthase inhibition in rats subjected to focal cerebral ischemia. Eur J Pharmacol. 2017;800:16-22.
72. Abdelsalam RM, Safar MM. Neuroprotective effects of vildagliptin in rat rotenone Parkinson's disease model: role of RAGE-NFkappaB and Nrf2-antioxidant signaling pathways. J Neurochem. 2015;133(5):700-7.

73. Smith MA, Taneda S, Richey PL, Miyata S, Yan SD, Stern D, et al. Advanced Maillard reaction end products are associated with Alzheimer disease pathology. Proc Natl Acad Sci U S A. 1994;91(12):5710-4.
74. Vitek MP, Bhattacharya K, Glendening JM, Stopa E, Vlassara H, Bucala R, et al. Advanced glycation end products contribute to amyloidosis in Alzheimer disease. Proc Natl Acad Sci U S A. 1994;91(11):4766-70.
75. Polykretis P, Luchinat E, Boscaro F, Banci L. Methylglyoxal interaction with superoxide dismutase 1. Redox Biol. 2020;30:101421.
76. Heneka MT, Carson MJ, El Khoury J, Landreth GE, Brosseron F, Feinstein DL, et al. Neuroinflammation in Alzheimer's disease. Lancet Neurol. 2015;14(4):388-405.

Supplementary Figure Legends

Additional file 1: Figure S1. Neuronal and endothelial NOS mRNA levels are reduced in early phase prion disease. mRNA levels of the neuronal NOS (a, *Nos1*) and endothelial NOS (b, *Nos3*) were reduced at 6 and 10 w.p.i. (*Nos1*: 6 w.p.i.: NBH: 1.0 ± 0.07, RML: 0.6 ± 0.04, P=0.0003, 10 w.p.i: NBH: 0.06 ± 0.03, RML: 0.4 ± 0.05, P=0.0183; *Nos3*: mRNA levels 6 w.p.i.: NBH: 1.0 ± 0.1, RML: 0.6 ± 0.6, P=0.0281; 10 w.p.i.: NBH: 1.3 ± 0.1, RML: 0.5 ± 0.1, P=0.0004) Data are presented as mean ± SEM, two-way ANOVA, *P<0.05, n=3-4 mice.

Additional file 2: Figure S2. Neuronal protein expression is reduced in prion disease. Proteins levels of MUNC 18, complexin 1/2, SNAP-25, and Kv3.1 are reduced in prion disease at 9 w.p.i.. Further proteins, including synaptobrevin, synaptophysin and synapsin, show tendencies for reduced expression levels in prion disease at 9 w.p.i.. Data are presented as mean ± SEM, n=9 NBH and n=6 RML mice. Some ratio calculations may use the same actin blots. Unpaired Student's *t*est, *P<0.05, ***P<0.001.

Additional file 3: Figure S3. a, immunocytochemistry of cortical regions from NBH, RML and RML+L-NAME treated mice showing cells staining for ICSM35 and DAPI. b, summary of relative number of cells possessing PrP^{Sc} positive signals (number of PrP positive cells/number of total cells (***P<0.001, unpaired Student's *t*-test). c, total number of cells counted under conditions indicated (one-way ANOVA, *P<0.05). Data are presented as mean ± SEM, n=3 NBH, n=3-5 RML and n=3 RML+L-NAME treated mice.

Figures

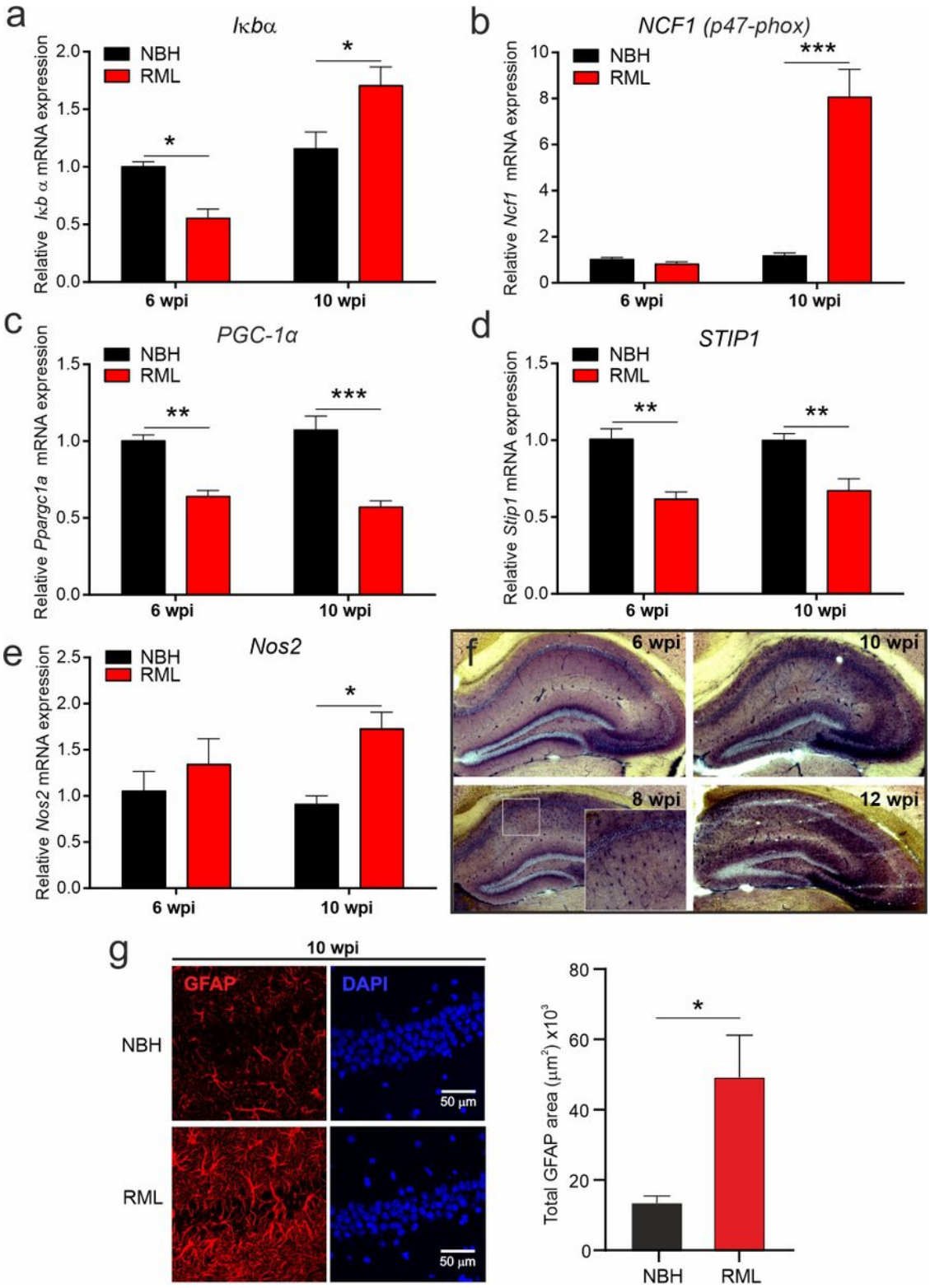

Figure 1

Neuroinflammation is enhanced early in prion disease. mRNA levels were determined at 6 and 10 w.p.i. in control (NBH) and prion infected (RML) mice for the following genes: I□b□ (a), NCF1 (b), PGC-1□ (c), STIP1 (d) and Nos2 (e). f, NADPH diaphorase staining of prion-inoculated brains (RML) at 6-12 w.p.i. shows enhanced signals in disease starting after 6 w.p.i. indicating enhanced NOS activity with strong signals in the CA1 and at later time points speeding across the whole hippocampus. g, immunocytochemistry

images show representative GFAP and DAPI staining in the hippocampus of NBH and RML mice at 10 w.p.i. (left) and GFAP signals expressed as absolute area (right). Data are presented as mean ± SEM, n=4 NBH and n=7 RML mice, two-way ANOVA (a-e) and unpaired Student's t-test (g) *P<0.05, **P<0.01, ***P<0.001.

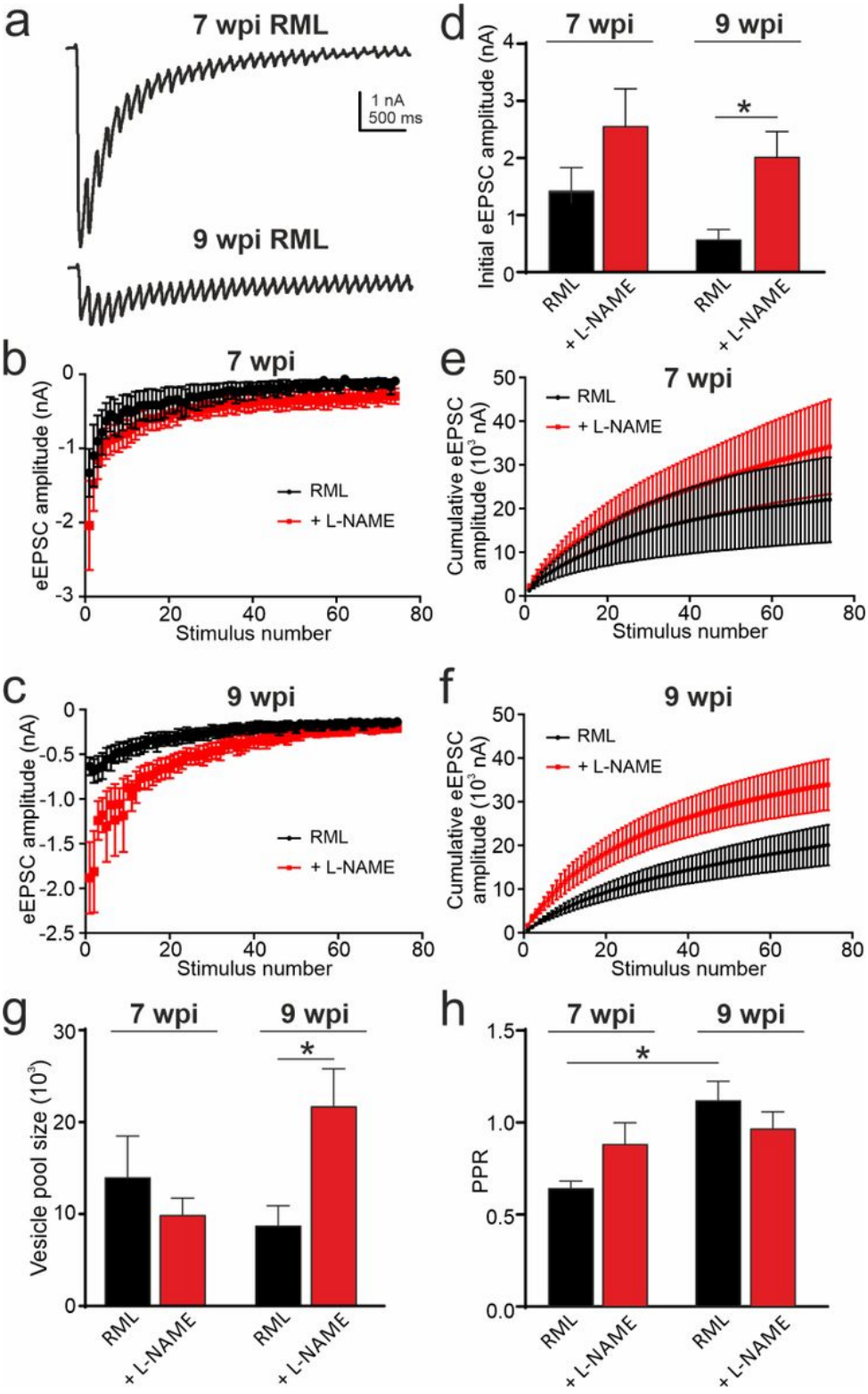

Figure 2

Decline in synaptic strength is recovered by NOS antagonism. Whole-cell patch clamp recordings showing hippocampal Schaffer collateral-evoked excitatory postsynaptic currents (eEPSC) from prion infected (vehicle treated RML, black) mice and RML mice treated with the NOS antagonists L-NAME (+L-NAME, red) for 3 weeks (9 w.p.i.). a, representative eEPSC trains recorded at 30 Hz for 10 s in an RML mouse at 7 w.p.i. and RML mouse at 9 w.p.i.. b and c, mean train eEPSC amplitudes at 7 and 9 w.p.i. for RML mice and RML mice following treatment. d, single eEPSC amplitudes at both time points for RML and treated RML mice. e and f, cumulative eEPSC amplitude plots at 7 and 9 w.p.i. for RML mice and RML mice following treatment. g, estimation of vesicle pool sizes at both time points for RML and treated RML mice. h, paired pulse ratios (PPR) at both time points for RML and treated RML mice. Data are presented as mean ± SEM, n=9 RML and n=6 RML+L-NAME treated mice with n=4-6 neurons per mouse, two-way ANOVA, *P<0.05.

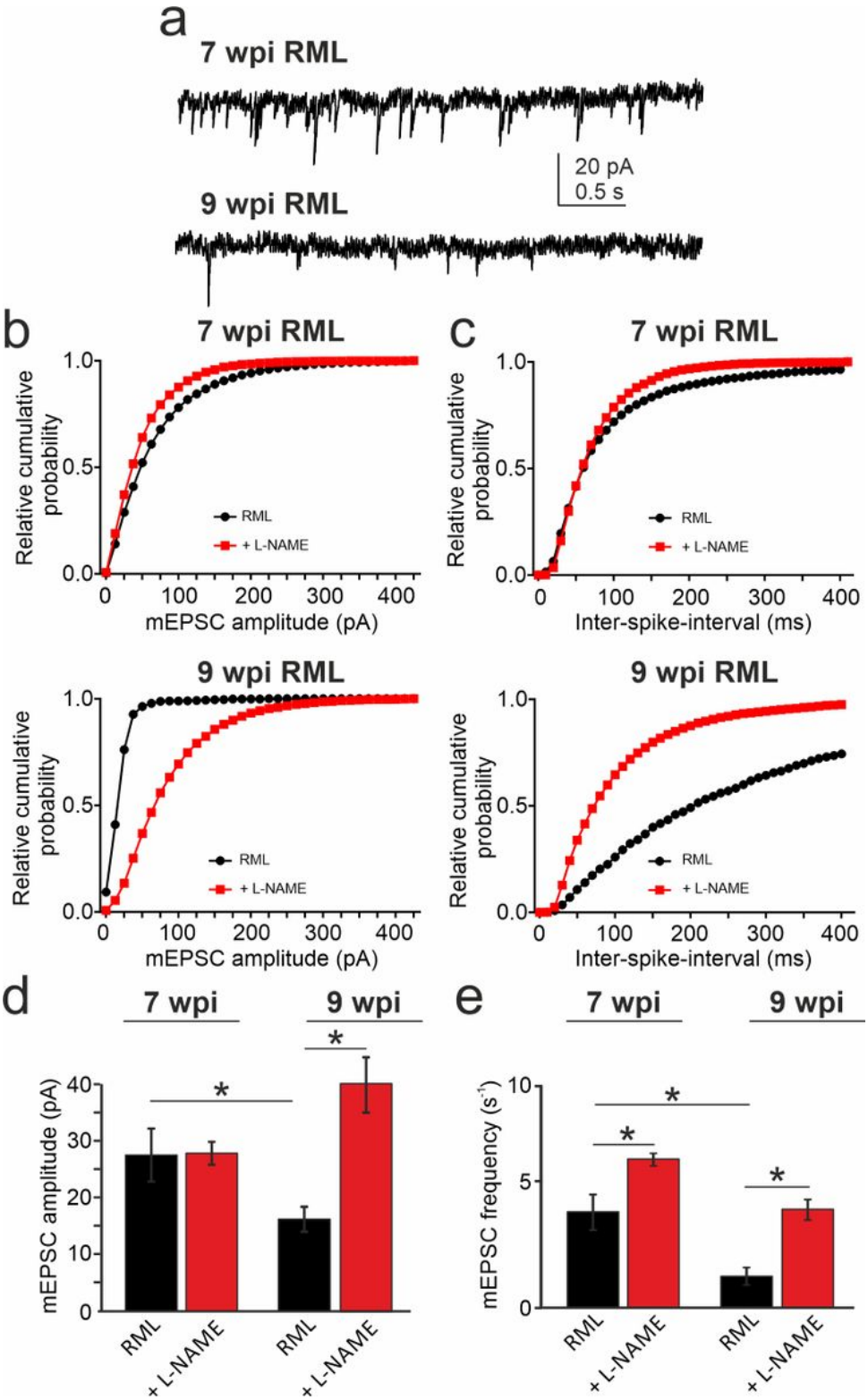

Figure 3

Spontaneous synaptic activity recovers following NOS antagonism at early time points. Spontaneous release measured as miniature excitatory postsynaptic currents (mEPSC) recovered following NOS inhibition. a, raw traces showing spontaneous release events for RML mice at indicated time points. b and c, relative cumulative probability diagrams shown for mEPSC amplitudes and inter-spike-intervals. L-NAME treatment results in a significant shift of the data distributions for both parameters (P<0.0001,

Kolmogorov-Smirnov test). d, mEPSC amplitudes and frequencies (e) show disease-dependent decline (black). L-NAME treatment reversed the reduction in mEPSC amplitudes and frequencies (red). Data are presented as mean ± SEM, n=9 RML and n=6 RML+L-NAME treated mice with n=4-6 neurons per mouse, one-way ANOVA, *P<0.05.

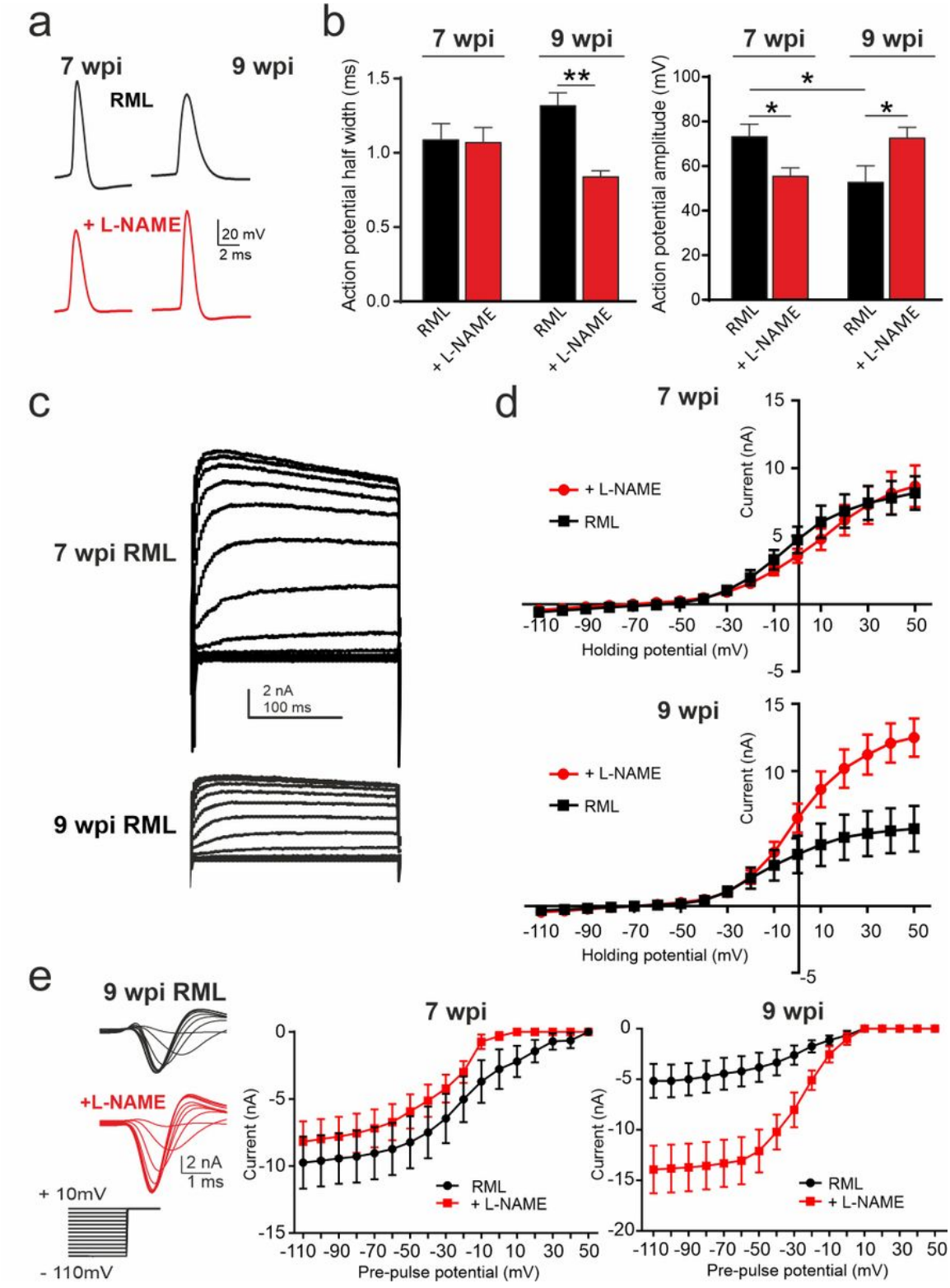

Figure 4

Postsynaptic neuronal health is protected by NOS antagonism. Pyramidal hippocampal neurons were characterised by whole-cell patch clamp. a, representative current-evoked action potentials. b, action potential half width and amplitudes were analysed at 7 and 9 w.p.i. and are shown for vehicle treated (black) and L-NAME treated RML (red) mice. c, voltage-gated potassium currents declined at 9 w.p.i. in RML mice (raw traces in c and current/voltage relationship [I/V, black] in d). L-NAME treatment prevents the decline in voltage-gated potassium currents at 9 w.p.i. (d, red). E, voltage-gated sodium currents decline at 9 w.p.i. in RML mice and L-NAME treatment (red) leads to enhanced currents at 9 w.p.i. (representative recordings at 9 w.p.i.). Data are presented as mean ± SEM, n=9 RML and n=6 RML+L-NAME treated mice with n=4-6 neurons per mouse, one-way ANOVA, *P<0.05, **P<0.01.

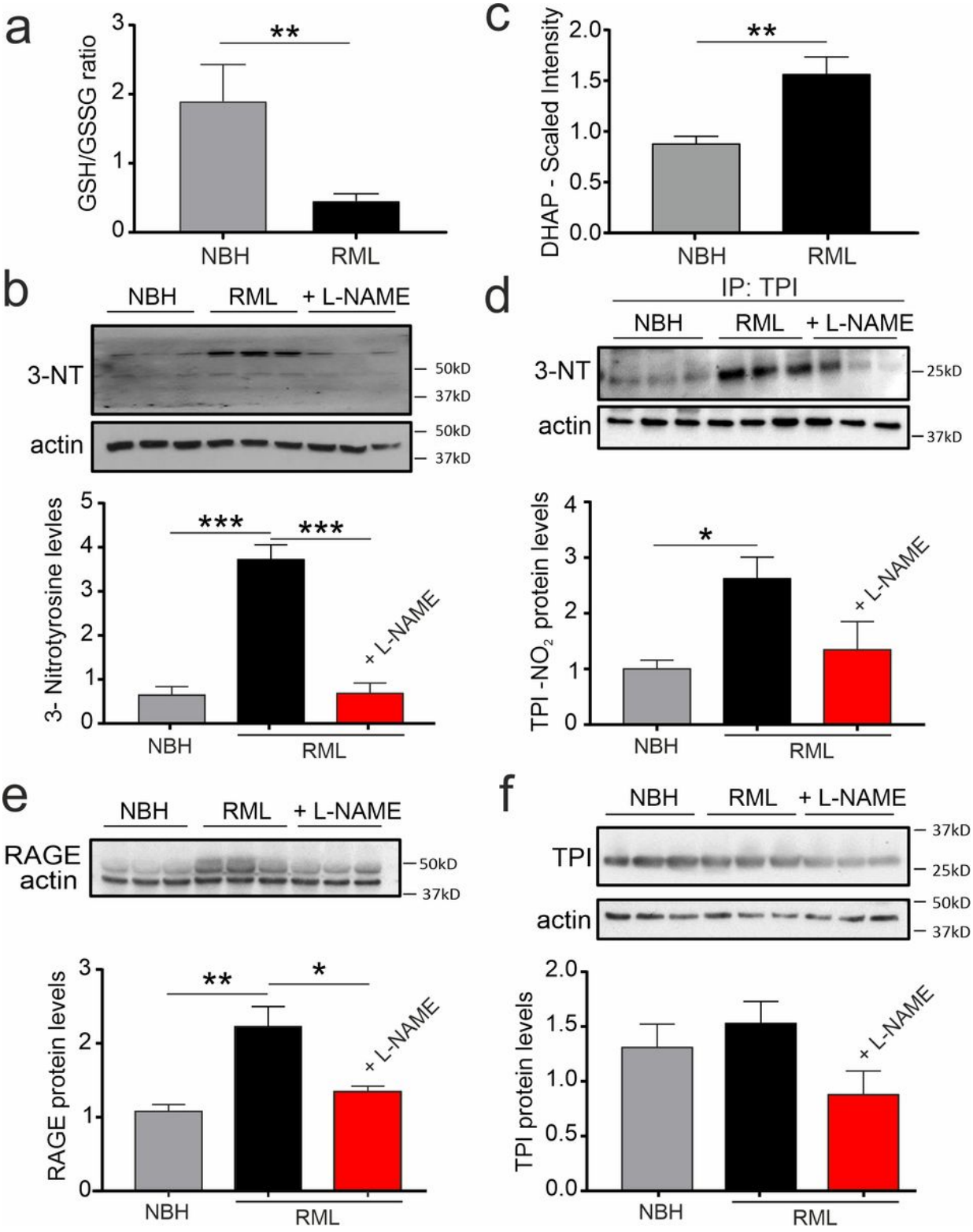

Figure 5

NOS inhibition reduces protein nitrotyrosination and glycation signalling. a, the ratio of reduced/oxidised glutathione is diminished in hippocampal tissue of RML mice at 10 w.p.i.. b, levels of 3-NT proteins is enhanced in RML mice and reduced to control levels (NBH) following L-NAME treatment. c, DHAP levels are increased in the hippocampus of RML mice. d, 3-NT formation of triose-phosphate isomerase (TPI) is increased in RML mice and reduced following L-NAME treatment. e, RAGE levels (upper band; lower band

represents actin) are enhanced in RML hippocampi and reduced following L-NAME treatment. f, total TPI levels are not affected by prion disease or treatment. Data are presented as mean ± SEM, n=6 NBH, n=9 RML mice (a, c) and n=3 mice each in b, d-f. Unpaired Student's t-test **P<0.01 (a, c), one-way ANOVA, *P<0.05 **P<0.01, ***P<0.001 (b, d-f).

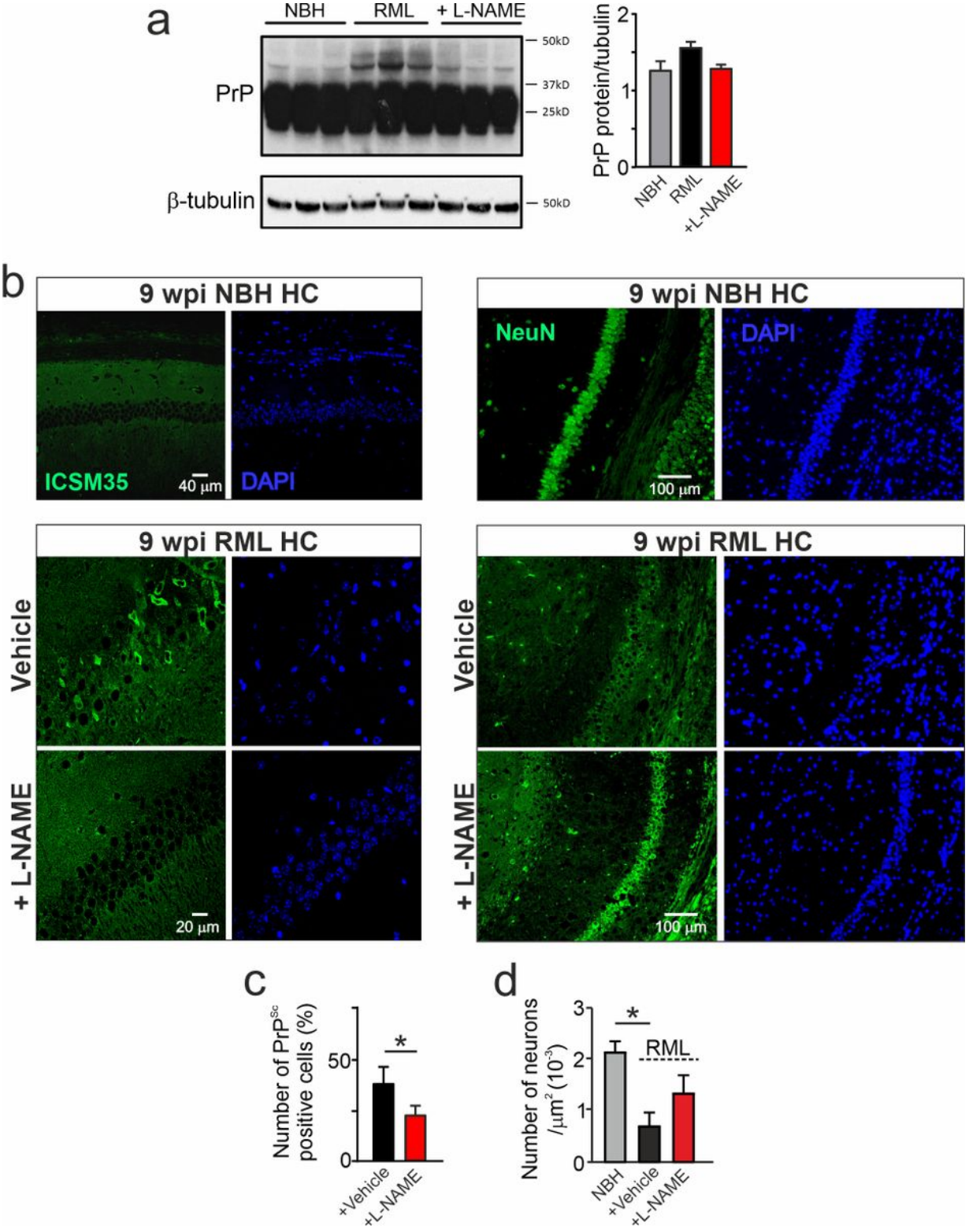

Figure 6

L-NAME treatment mitigates prion protein misfolding and reduces cell death in RML mice. a, immunoblotting for prion protein in the hippocampus (HC) from control mice (NBH), prion-diseased mice (RML) and RML mice treated with L-NAME at 9 w.p.i.. b, left: immunocytochemistry of hippocampal regions from NBH, RML and RML+L-NAME treated mice showing pyramidal neurons (staining ICSM35+DAPI). Right: immunocytochemistry of hippocampal regions from NBH, RML and RML+L-NAME treated mice showing pyramidal neurons (staining NeuN+DAPI). c, summary of relative number of cells possessing PrPSc positive signals (number of PrP positive cells/number of total cells) in the hippocampal CA1 region (*P<0.05, unpaired Student's t-test). d, total number of pyramidal neurons counted in hippocampal CA1 region under conditions indicated (one-way ANOVA, *P<0.05). Data are presented as mean ± SEM, n=3 NBH, n=3-5 RML and n=3 RML+L-NAME treated mice.

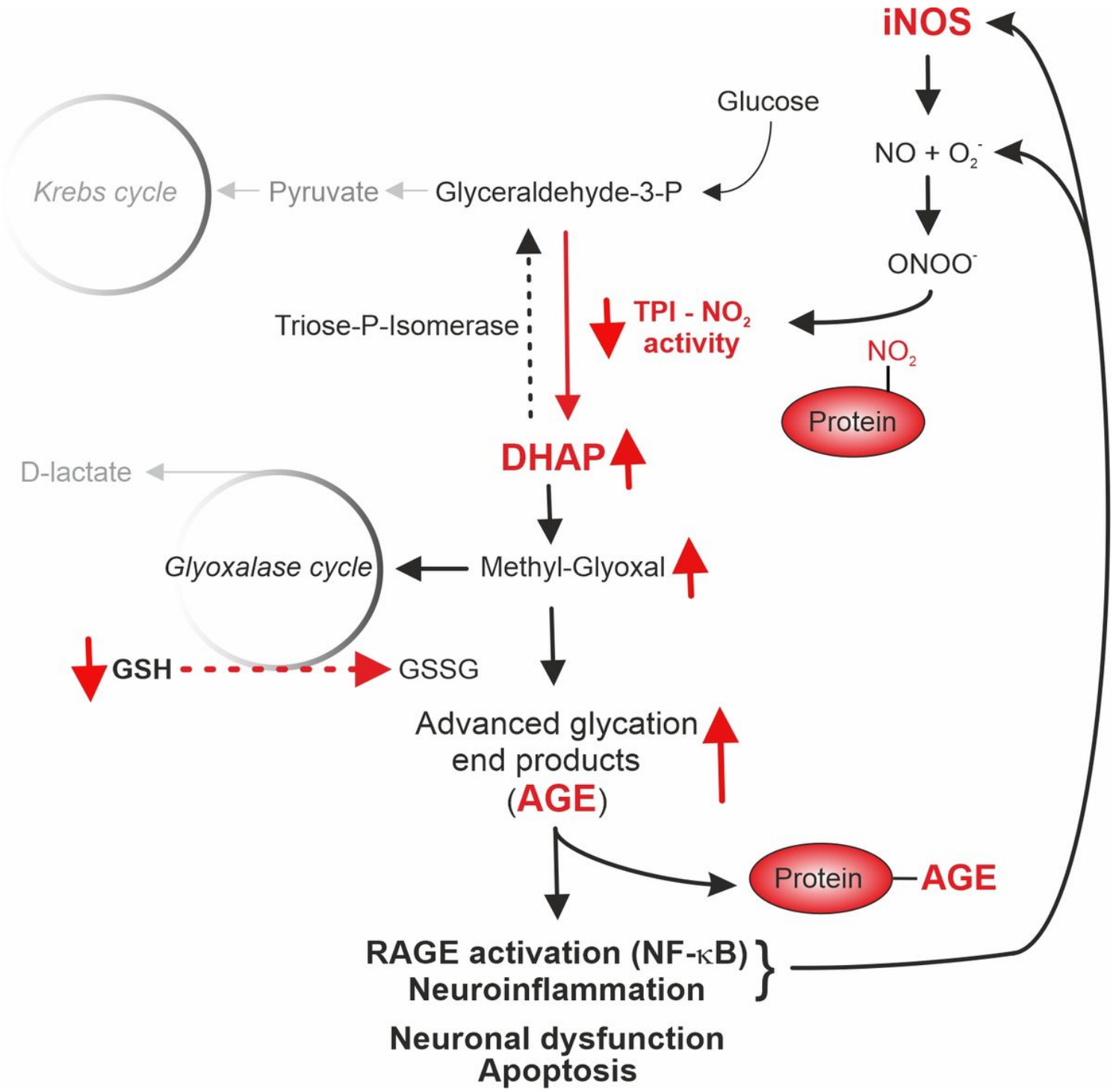

Figure 7

Schematic representation of the pathways impacted on by excessive protein nitrotyrosination. Glycolysis generates glutaraldehyde-3-phosphate (G3P) that the enzyme triose phosphate isomerase (TPI) uses to form dihydroxyacetone (DHAP) which spontaneously and non-enzymatically decomposes to methylglyoxal. The glyoxalase cycle is the detoxification system by which methylglyoxal is transformed into lactate using glutathione (GSH) as a cofactor. Following activation of iNOS associated with enhanced levels of NO and peroxynitrite, 3-nitrotyrosination of TPI decreases its activity, which leads to an accumulation of DHAP and methylglyoxal. However, high concentrations of methylglyoxal will

overload this clearance mechanism, leading to an accumulation of GSSG and the formation of advanced glycation end products (AGE) with subsequent activation of the receptors for AGE (RAGE). Under pathological conditions, glycated proteins are compromised and can aggregate which further contributes to inflammation and cell dysfunction.

Supplementary Files

This is a list of supplementary files associated with this preprint. Click to download.

- Suppfig1.jpg
- Suppfig3.jpg
- Suppfig2.jpg